Origin of profuse {11$\bar{2}$1} deformation twins in Mg-Gd alloys

Cong He[a], Zhiqiao Li[a], Dehao Kong[a], Xiaojun Zhao[a], Houwen Chen[a,b,c,*], Jian-Feng Nie[d*]

[a] International Joint Laboratory for Light Alloys (Ministry of Education), College of Materials Science and Engineering, Chongqing University, Chongqing 400044, China
[b] Shenyang National Laboratory for Materials Science, Chongqing University, Chongqing 400044, China
[c] Electron Microscopy Center, Chongqing University, Chongqing 400044, China
[d] Department of Materials Science and Engineering, Monash University, Victoria 3800, Australia

*Corresponding authors
hwchen@cqu.edu.cn (Houwen Chen), jianfeng.nie@monash.edu (Jian-Feng Nie)

Abstract

Deformation twins in Mg–Gd alloys are investigated. It is found that the dominant twinning mode switches from {10$\bar{1}$2} twinning to {11$\bar{2}$1} twinning, with an increase in the Gd concentration in Mg. Our first-principles calculations suggest that the formation of the {11$\bar{2}$1} twin in the Gd-rich alloy is triggered by the reduced {11$\bar{2}$1} twin boundary energy, which results from strain relaxation along the twin boundary. Furthermore, this twinning mode is suggestive to be activated in other Mg alloys with a high concentration of solute atoms having larger size than Mg.

Keywords: Deformation twins; Mg alloys; Twin boundary; First-principles calculations.

Basal <a> slip is widely accepted as the primary deformation mode at ambient temperature to accommodate the strain parallel to the *a*-axis in hexagonal Mg and its alloys during plastic deformation. However, this slip mode alone cannot provide five independent slip systems to satisfy von Mises criterion to undergo homogeneous deformation [1]. Twinning thus acts as one of the supplementary deformation modes to accommodate the strain along the *c*-axis. Besides, twinning also plays an important role in texture evolution during recrystallization [2, 3], and in crack nucleation [4]. Therefore, a better understanding of the twinning process, including the origins of different twinning modes, is important.

For pure Mg, the commonly observed twinning modes include {10$\bar{1}$1}<$\bar{1}$012>, {10$\bar{1}$2}<$\bar{1}$011> and {10$\bar{1}$3}<$\bar{3}$032> systems, where {10$\bar{1}$2}<$\bar{1}$011> twinning is most frequent [5-9]. While {11$\bar{2}$1} deformation twin has been detected in close-packed hexagonal (HCP) pure Zr [10], Ti [11] and Co [12, 13] metals, it has never been experimentally observed in pure Mg. This fact seems to indicate that twinning on the {11$\bar{2}$1} plane of pure Mg is not favorable. However, in an early study [14], Eckelmeyer *et al.* detected this twining mode in a Mg–9wt%Y alloy using Laue back reflection X-ray technique. Later, this twinning mode was confirmed by electron backscattered diffraction (EBSD) analysis in WE54 alloy [15] and a Mg–Gd–Al alloy containing long-period stacking-ordered (LPSO) structures [16]. However, all these studies merely reported the occurrence of this twinning mode and its effect on mechanical behaviors, none of them explored the origin of this deformation mode. Recently, Stanford *et al.* [17] examined twinning behaviors in Mg–5wt%Y and Mg–10wt%Y alloys. They found that {11$\bar{2}$1} twin formed only in the Mg–10wt%Y alloy. They ascribed the formation of such twin to the effect of higher Y concentration on the stress to active different twinning modes, i.e.,

the stress to activate twinning on $\{10\bar{1}2\}$ plane was increased substantially but that on $\{11\bar{2}1\}$ plane remained nearly unchanged, leading to the dominanting twinning mode of $\{11\bar{2}1\}$ in Mg–10wt%Y. However, this hypothesis has not been verified by any direct experimental evidence yet. The purpose of this paper is to report experimental observations on the increased volume fraction of $\{11\bar{2}1\}$ twin in Mg alloys with increasing Gd content and its origin of this phenomenon.

Pure Mg, Mg–6wt%Gd (Mg–1.0at%Gd) and Mg–14wt%Gd (Mg–2.5at%Gd) alloys, used in the present study, were produced by melting pure metals and casting under a protective atmosphere. Rectangular plates with 75 mm × 55 mm × 15 mm dimension were cut from the cast ingots, and solution heated for 48 hours at 500 °C for Mg–6Gd and Mg–14Gd alloys. To avoid quenching cracks, all solution treated samples were quenched into hot water of ~60 °C. Samples of pure Mg, Mg–6Gd and Mg–14Gd alloys were then hot-rolled by ~35% thickness reduction at 300 °C, 450 °C and 500 °C, respectively. To acquire a uniform grain size, hot-rolled specimens of pure Mg, Mg–6Gd and Mg–14Gd alloys were respectively heat treated at 400 °C, 450 °C and 500 °C for 30 min, followed by ~60 °C hot water quenching. The obtained grain sizes are similar, ~60 μm for pure Mg, ~75 μm for Mg–6Gd, and ~60 μm for Mg–14Gd. Small rectangular bars with a dimension of 7 mm (transverse direction: TD) × 8 mm (normal direction: ND) ×10 mm (rolling direction: RD) were machined from the hot-rolled plates and subsequently compressed by ~3% along RD with a strain rate of 10^{-3} s^{-1} at ambient temperature. Specimen surface for EBSD mapping, perpendicular to RD, was electrochemically polished in the AC2 electrolyte. The microstructure of the compression-deformed sample was examined by EBSD, using a TESCAN MIRA3 scanning electron microscopy equipped with an Oxford AZtec EBSD detector. Thin foils for transmission electron microscopy observations were prepared by ion-milling using Gatan PIPS 695 at -70 °C and characterized using a Cs-corrected FEI Titan G2 60–300 ChemiSTEM operated at 300 kV.

First-principles calculations were performed using the Vienna *ab initio* Simulation Package (VASP) code [18] with generalized gradient approximation of Perdew-Burke-Ernzerhof (GGA-PBE) [19]. The *k*-space sampling was implemented by the setting of 18 × 18 × 12 in the optimization of Mg unit cell and the *k*-point mesh used in the later calculations was adjusted according to the supercell size. The cut-off energy of 400 eV was tested to bring accurate-enough results and applied in all simulations. The convergence criteria were set as 10^{-6} eV in electron self-constituent relaxations and 10^{-2} eV/Å in force. The special quasi-random structure (SQS) [20-22] approach was applied here to simulate the random distribution of solute atoms in Mg solid solution. In this work, all the involved SQS supercells were generated using the *mcsqs* module in alloy theoretic automated toolkit (ATAT) package [23]. The atomic local strain invariant (ALSHI) was computed by following the definition in Ref. [24] and the calculation details are the same as those described in Ref. [5].

The EBSD orientation map in Fig. 1a shows copious twin lamellas that have formed in pure Mg compressed by 2.8%. In an enlarged image, shown in Fig. 1b, twin chains and the twin-twin transfer phenomenon [25] are both visible. In the histogram of the misorientation angle distribution shown in Fig. 1c, corresponding to Fig. 1a, the relative frequency of these grain boundaries peaks at the misorientation angle of ~86° and the corresponding misorientation axis is $<11\bar{2}0>$. This indicates that the twin lamellas, as enclosed by red lines inside grains in Fig. 1a, are $\{10\bar{1}2\}$ twins. This observation is consistent with previous results on deformed pure Mg [26, 27]. Figures 1d-1f show the results from the deformed Mg–6Gd alloy. According to the statistic analysis in Fig. 1f, there are two peaks in the histogram: one at ~86° and the other at ~34°. The misorientation axis is $<11\bar{2}0>$ for the former and $<1\bar{1}00>$ for the later. Based on the crystallographic information above, these two types of boundaries are readily identified as $\{10\bar{1}2\}$ and $\{11\bar{2}1\}$ twin boundaries (TBs), as marked by red lines and yellow lines in Figs. 1d and 1e. The number of $\{11\bar{2}1\}$ TBs is much less than that of $\{10\bar{1}2\}$. With a further

increase in the Gd content to 14wt%, $\{11\bar{2}1\}$ TB is more frequently detected, and its number density is even higher than that of $\{10\bar{1}2\}$, Figs. 1g and 1h. This leads to the occurrence of two distinct peaks at ~86° and ~34° (Fig. 1i) which correspond to $\{10\bar{1}2\}$ and $\{11\bar{2}1\}$ TBs, respectively. Our EBSD results indicate that, with an increase in the Gd content in Mg, the relative frequency of $\{11\bar{2}1\}$ TB is significantly enhanced.

Figure 2a shows one such twin lamella, with a relatively small twin thickness of ~450 nm. Figure 2b displays the selected area electron diffraction (SAED) pattern recorded from the region enclosed by a blue rectangular frame in Fig. 2a. Further analysis reveals that the twin lattice has anticlockwise rotated ~34° about $<1\bar{1}00>$, Fig. 2c. Figure 2d shows the atomic-scale structure of the $\{11\bar{2}1\}$ coherent TB in Fig. 2a. The corresponding twinning elements are deduced as: K_1: $\{11\bar{2}1\}$, K_2: $\{0001\}$, η_1: $<\bar{1}\bar{1}26>$, η_2: $<11\bar{2}0>$ and s = 0.616 [28]. This twin relationship is consistent with the result made from EBSD, Fig. 1. Figure 2e shows the schematic diagram of the $\{11\bar{2}1\}$ TB based on the structure in Fig. 2d. According to a previous study [4], this TB has a 2-fold rotation axis of symmetry in the η_1 ($<\bar{1}\bar{1}26>$) direction rather than a mirror plane in K_1 ($\{11\bar{2}1\}$), which corresponds to type II twin accoring to the classic definition of twins [4, 29, 30]. The stacking sequences are ⋯ABAB⋯ for the matrix and ⋯ACAC⋯ for the twin [31], Fig. 2e.

To reveal the physical origin of the formation of $\{11\bar{2}1\}$ twin in the Mg–Gd alloys but not in pure Mg, first-principles calculations were performed. Structure of the relaxed supercells used in this work agrees well with previous results [30, 31]. The SQS approach was applied here to randomly distribute Gd atoms in the Mg solid solution. Figure 3a shows the energy variation of the $\{11\bar{2}1\}$ and $\{10\bar{1}2\}$ TBs in the Mg–Gd alloys. Unexpectedly, alloying with Gd leads to a significant drop in the value of $\{11\bar{2}1\}$ TB energy (γ_t): the higher the Gd content in Mg, the lower the value. For Mg–2.5at%Gd and Mg–5.0at%Gd alloys, the calculated γ_t value of $\{11\bar{2}1\}$ TB decreases from 123 mJ/m^2 to 109 mJ/m^2 and 69 mJ/m^2, respectively. However, with the increasing Gd concentration in the α-Mg, the γ_t value of $\{10\bar{1}2\}$ TB remains nearly the same as that in pure Mg.

To understand why Gd atoms in the α-Mg solid solution can decrease the $\{11\bar{2}1\}$ TB energy, we calculated the ALSHI in $\{11\bar{2}1\}$ TB of Mg_{160} (Fig. 3b), $Mg_{158}Gd_2$ (Fig. 3c) and $Mg_{156}Gd_4$ (Fig. 3d). It is found that large extension strains are distributed along the TB in pure Mg (Fig. 3b), but that the strain is substantially reduced when the Gd concentration is increased, especially in the $Mg_{156}Gd_4$ (Mg–14wt%Gd) alloy, Figs. 3c and 3d. It is apparent that the higher Gd concentration in the α-Mg solid solution significantly minimizes the elastic strains along the $\{11\bar{2}1\}$ TB and thus the TB energy.

To date, twin nucleation mechanisms in HCP metals include homogeneous and heterogeneous nucleations. In both nucleation modes, it has been reported that, from an energy point of view, the activation energy for twin nucleation depends sensitively on the TB energy, i.e., when the TB energy is lower, it is much easier to generate a stable twin nucleus of a critical size, thus promoting the twin nucleation [32, 33]. In this study, alloying Mg with Gd results in a significant reduction of $\{11\bar{2}1\}$ TB energy in the Mg–Gd alloys (Fig. 3), which would facilitate the formation of a stable twin nucleus. In this sense, the propensity for nucleating a $\{11\bar{2}1\}$ twin in a Mg–Gd alloy is expected to be increased when compared with the situation in pure Mg, and therefore the reduction of $\{11\bar{2}1\}$ twin boundary energy may contribute to the formation of profuse $\{11\bar{2}1\}$ twins in the Mg–14Gd alloy (Fig. 1). Such correlation has been previously reported in Re–10at%W [22] and Zr–2.2wt%Hf alloys [34]. It is to be noted that kinetics may also play an important role in the twin formation [35]. Our first-principles calculation only provides an energetic analysis but neglects the contributions of two kinetic factors, the effect of Gd atoms on the motion of twinning dislocations on different types of twin planes and the potential facilitation of twin nucleation by dissociation of <c + a> dislocations. The former

requires more research in the future, since models are still not available for performing a quantitative comparison of the magnitudes of shuffle involved in twinning dislocations for different types of twinning modes. The latter could be another reason why plentiful $\{11\bar{2}1\}$ twins are activated in Mg–Gd alloys. It has been reported that <c + a> dislocations form readily in rare-earth-containing Mg alloys [36]. According to previous studies based on molecular dynamics simulations [37, 38], the dissociation of a <c + a> dislocation would more likely favor the formation of $\{11\bar{2}1\}$ twin rather than $\{10\bar{1}2\}$ twin (under an applied stress 140 MPa vs. 500 MPa). Some *in-situ* TEM work is needed in the future to experimentally determine whether $\{11\bar{2}1\}$ twin can be nucleated by <c + a> dislocation dissociation in the Mg–14wt%Gd alloy.

It has been reported that $\{11\bar{2}1\}$ twins forms frequently in HCP pure Zr [10], Ti [11] and Co [12, 13] metals but not in pure Mg [26, 27]. Note that all HCP metals that exhibit $\{11\bar{2}1\}$ twinning mode have a *c*/*a* ratio smaller than the ideal value 1.633. However, pure Co and pure Mg have nearly the same *c*/*a* ratio but exhibit different twinning behaviors, i.e., $\{11\bar{2}1\}$ twinning occurs in Co but not in Mg, Fig. 1a. Therefore, a *c*/*a* ratio smaller than 1.633 alone does not result in the formation of $\{11\bar{2}1\}$ twins in HCP metals. In an early report, Crocker and Bevis [39] attributed the formation of $\{11\bar{2}1\}$ twins in HCP Ti and Zr metals to the simpler shear (each point of the Bravais lattice is sheared to its correct twin position) and the smaller shuffle during the twinning process. However, this explanation cannot rationalize why $\{11\bar{2}1\}$ twinning does not activate in pure Mg, considering that the shear and the shuffle involved for $\{11\bar{2}1\}$ twinning in pure Mg is nearly the same as that in HCP Ti and Zr.

Although $\{11\bar{2}1\}$ twinning mode does not operate in pure Mg, it can form in some Mg alloys, such as Mg–Y alloys [14, 15, 17] and Mg–Gd–Al [16]. Stanford *et al*. [17] detected $\{11\bar{2}1\}$ twins in a Mg–10wt%Y alloy. To rationalize their observation, they hypothesesd that $\{11\bar{2}1\}$ twinning is much less sensitive to Y concentration than $\{10\bar{1}2\}$ twinning, thus leading to an increased critical resolved shear stress (CRSS) for $\{10\bar{1}2\}$ twinning and a nearly unchanged CRSS for $\{11\bar{2}1\}$ twinning. In the present study, $\{11\bar{2}1\}$ twinning is unambiguously activated in the Mg–6Gd and Mg–14Gd alloys, Figs. 1 and 2. Based on first-principles calculations, we correlate the activation of $\{11\bar{2}1\}$ twin modes in the Mg–Gd alloys with the reduced TB energy, from an energy point of view. Gd atoms in the α-Mg solid solution can significantly affect the TB energy of $\{11\bar{2}1\}$ but not $\{10\bar{1}2\}$, Fig. 3a. The reduction of $\{11\bar{2}1\}$ TB energy, indicates a lower energy barrier to nucleate such deformation twin. This leads to profuse formation of $\{11\bar{2}1\}$ twin in the Mg–Gd alloys. Our calculation results, Fig. 4a, further suggest that other solutes having larger atomic size than Mg, such as Er, Y or Nd, can also decrease the $\{11\bar{2}1\}$ TB energy and thus this twinning mode is also expected to activate and play an important role in the plastic deformation of Mg alloys containing a higher concentration of such alloying elements. In contrast, solutes with atomic size smaller than Mg, such as Zn or Al, remarkably enhance the $\{11\bar{2}1\}$ TB energy (Fig. 4b). This may be the reason why $\{11\bar{2}1\}$ twins are never observed in AZ31, AZ80, AZ81 or ZK60 alloy.

In summary, $\{11\bar{2}1\}$ twinning does not occur in pure Mg but takes place in Mg–Gd alloys. The number density of the $\{11\bar{2}1\}$ twin increases with the Gd content in the α-Mg solid solution. From an energy point of view, the formation of $\{11\bar{2}1\}$ twins in the Mg–Gd alloys is intimately related to the decrease of $\{11\bar{2}1\}$ TB energy with increasing Gd concentration. This reduction is caused by relaxation of elastic strains along the $\{11\bar{2}1\}$ TB. Some other solutes that have larger atomic size than Mg are also found to have this effect, indicating that $\{11\bar{2}1\}$ twinning can be ubiquitous in Mg alloys containing a high concentration of such larger solute atoms.

Acknowledgments

This work is financially supported by National Natural Science Foundation of China (51771036, 51131009 and 51421001), National Key Research and Development Program of China (2016YFB0700402). Cong He also gratefully acknowledges the facility access provided by the Electron Microscopy Center in Chongqing University.

Disclosure statement

No potential conflict of interest was reported by the authors.

References

[1] G. Proust, C.N. Tomé, A. Jain, S.R. Agnew, Int. J. Plast. 25 (2009) 861.
[2] Y. Xin, X. Zhou, Q. Liu, Mater. Sci. Eng. A 567 (2013) 9.
[3] D. Guan, W.M. Rainforth, L. Ma, B. Wynne, J. Gao, Acta Mater. 126 (2017) 132.
[4] J.W. Christian, S. Mahajan, Prog. Mater. Sci. 39 (1995) 1.
[5] J.F. Nie, Y.M. Zhu, J.Z. Liu, X.Y. Fang, Science 340 (2013) 957.
[6] Y.M. Zhu, S.W. Xu, J.F. Nie, Acta Mater. 143 (2018) 1.
[7] H. Zhou, G.M. Cheng, X.L. Ma, W.Z. Xu, S.N. Mathaudhu, Q.D. Wang, Y.T. Zhu, Acta Mater. 95 (2015) 20.
[8] J. Wang, S.K. Yadav, J.P. Hirth, C.N. Tomé, I.J. Beyerlein, Mater. Res. Lett. 1 (2013) 126.
[9] R.C. Pond, J.P. Hirth, A. Serra, D.J. Bacon, Mater. Res. Lett. 4 (2016) 185.
[10] P.A. Juan, C. Pradalier, S. Berbenni, R.J. McCabe, C.N. Tomé, L. Capolungo, Acta Mater. 95 (2015) 399.
[11] S. Jin, K. Marthinsen, Y. Li, Acta Mater. 120 (2016) 403.
[12] K.G. Davis, E. Teghtsoonian, Acta Metall. 10 (1962) 1189.
[13] Y.T. Zhu, X.Y. Zhang, H.T. Ni, F. Xu, J. Tu, C. Lou, Mater. Sci. Eng. A 548 (2012) 1.
[14] K.H. Eckelmeyer, R.W. Hertzberg, Metall. Trans. 1 (1970) 3411.
[15] N. Stanford, Phil. Mag. Lett. 88 (2008) 379.
[16] K. Kishida, A. Inoue, H. Yokobayashi, H. Inui, Scr. Mater. 89 (2014) 25.
[17] N. Stanford, R.K.W. Marceau, M.R. Barnett, Acta Mater. 82 (2015) 447.
[18] G. Kresse, J. Furthmüller, Phys. Rev. B 54 (1996) 11169.
[19] J.P. Perdew, K. Burke, M. Ernzerhof, Phys. Rev. Lett. 77 (1996) 3865.
[20] A. Zunger, S.H. Wei, L.G. Ferreira, J.E. Bernard, Phys. Rev. Lett. 65 (1990) 353.
[21] C. Jiang, C. Wolverton, J. Sofo, L.-Q. Chen, Z.-K. Liu, Phys. Rev. B 69 (2004) 214202.
[22] M. de Jong, J. Kacher, M.H.F. Sluiter, L. Qi, D.L. Olmsted, A. van de Walle, J.W. Morris, A.M. Minor, M. Asta, Phys. Rev. Lett. 115 (2015) 065501.
[23] A. van de Walle, P. Tiwary, M. de Jong, D.L. Olmsted, M. Asta, A. Dick, D. Shin, Y. Wang, L.Q. Chen, Z.K. Liu, Calphad 42 (2013) 13.
[24] J. Li, Modell. Simul. Mater. Sci. Eng. 11 (2003) 173.
[25] C. Guo, R. Xin, C. Ding, B. Song, Q. Liu, Mater. Sci. Eng. A 609 (2014) 92.
[26] Q. Yu, J. Wang, Y. Jiang, R.J. McCabe, C.N. Tomé, Mater. Res. Lett. 2 (2013) 82.
[27] S. Yi, I. Schestakow, S. Zaefferer, Mater. Sci. Eng. A 516 (2009) 58.
[28] M.H. Yoo, Metall. Trans. A 12 (1981) 409.
[29] H.A. Khater, A. Serra, R.C. Pond, Phil. Mag. 93 (2013) 1279.
[30] O. MacKain, M. Cottura, D. Rodney, E. Clouet, Phys. Rev. B 95 (2017) 134102.

[31] N.J. Lane, S.I. Simak, A.S. Mikhaylushkin, I.A. Abrikosov, L. Hultman, M.W. Barsoum, Phys. Rev. B 84 (2011) 184101.
[32] L. Capolungo, I.J. Beyerlein, Phys. Rev. B 78 (2008) 024117.
[33] M.H. Yoo, J.K. Lee, Phil. Mag. A 63 (1991) 987.
[34] M.H. Yoo, J.R. Morris, K.M. Ho, S.R. Agnew, Metall. Mater. Trans. A. 33 (2002) 813.
[35] J. Wang, I.J. Beyerlein, C.N. Tomé, Scr. Mater. 63 (2010) 741.
[36] S. Sandlöbes, Z. Pei, M. Friák, L.F. Zhu, F. Wang, S. Zaefferer, D. Raabe, J. Neugebauer, Acta Mater. 70 (2014) 92.
[37] T. Nogaret, W.A. Curtin, J.A. Yasi, L.G. Hector, D.R. Trinkle, Acta Mater. 58 (2010) 4332.
[38] M. Ghazisaeidi, W.A. Curtin, Modell. Simul. Mater. Sci. Eng. 21 (2013) 055007.
[39] A.G. Crocker, M. Bevis, in: R.I. Jaffee, N.E. Promisel (Eds.), The Science, Technology and Application of Titanium, Pergamon, 1970, pp. 453.

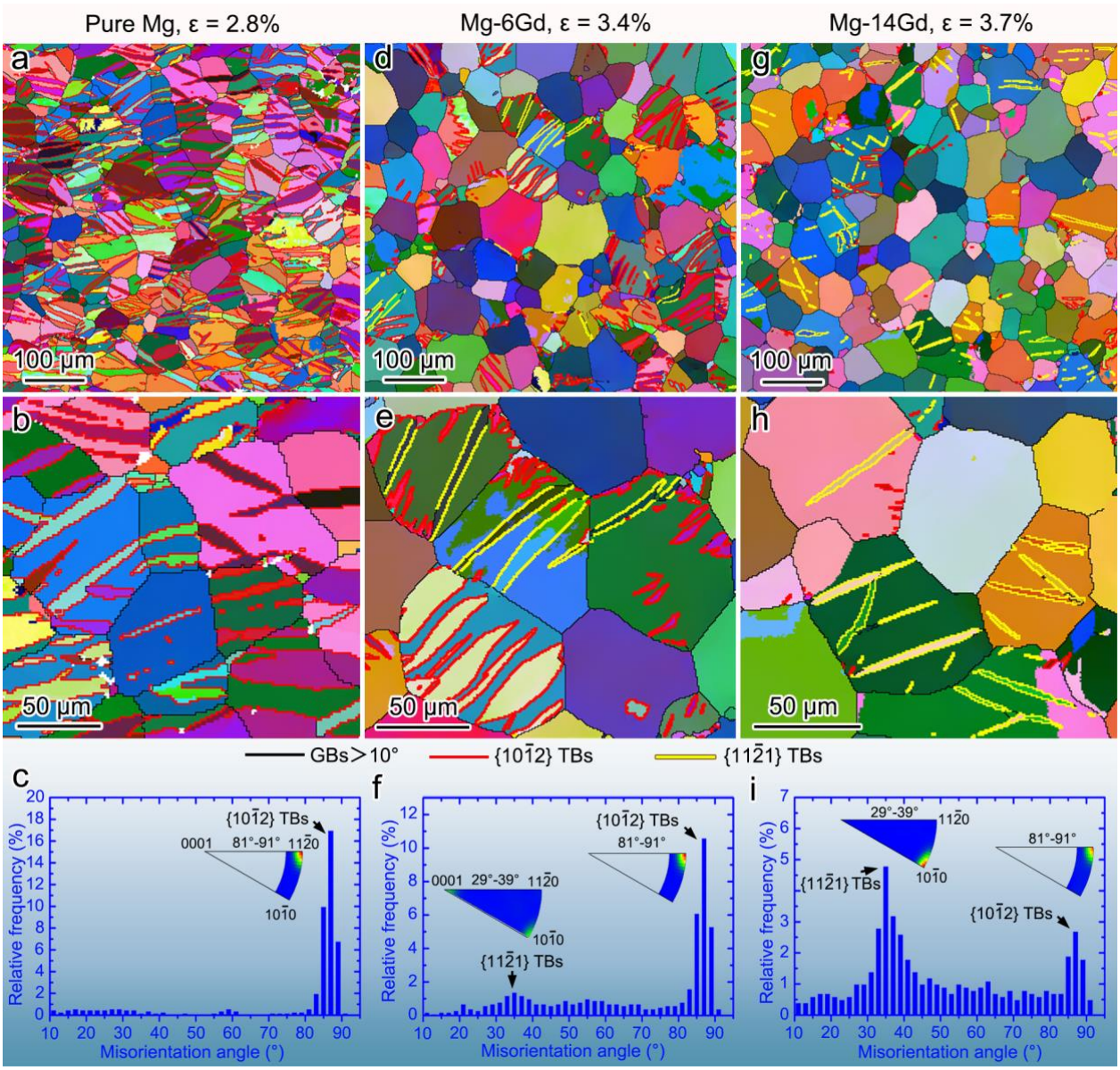

Fig. 1. EBSD maps of compression-deformed samples of (a-c) pure Mg, (d-f) Mg–6Gd, and (g-i) Mg–14Gd. The enlarged EDSB orientation maps of (a), (d), and (g) are shown in (a), (e) and (h), respectively. (c), (f) and (i) show the misorientation angle and misorientation axis distributions corresponding to (a), (d) and (g), respectively. The samples shown were compressed at room temperature by 2.8% for pure Mg, 3.4% for Mg–6Gd and 3.7% for Mg–14Gd. Black, red and yellow lines represent general grain boundaries, {10$\bar{1}$2} TBs and {11$\bar{2}$1} TBs, respectively.

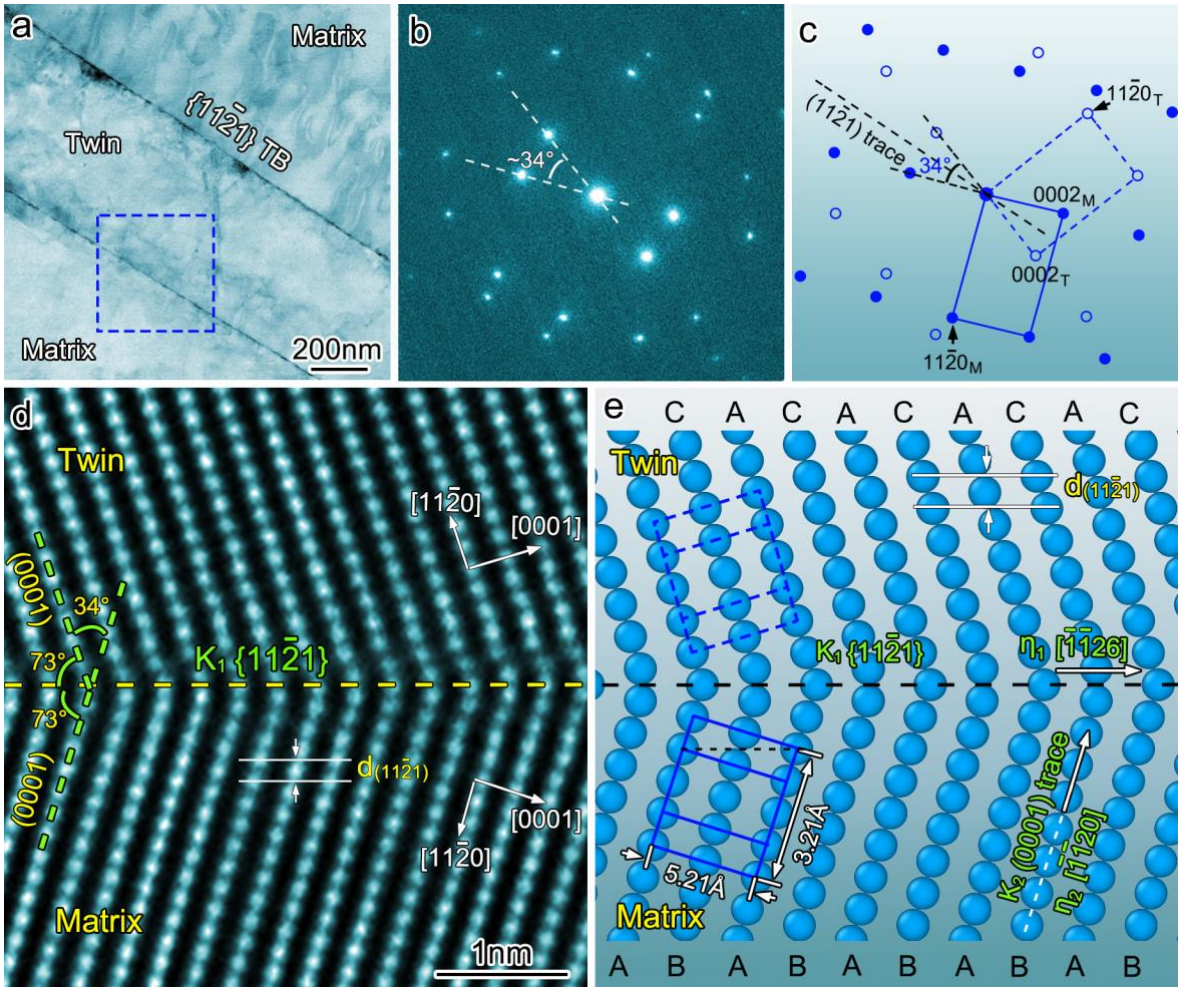

Fig. 2. (a) Low-magnification bright-field scanning transmission electron microscopy (BF-STEM) image of a {11$\bar{2}$1} twin in Mg–14Gd alloy after 3.8% compression. (b) SAED pattern corresponding to the area marked by the blue dashed-line square frame in (a), with electron beam direction parallel to <1$\bar{1}$00>. (c) Schematic diagram of the SEAD pattern in (b). The SAED patterns of the matrix and the twin are rotated by ~34° around <1$\bar{1}$00> axis, with {11$\bar{2}$1} as the twin plane. (d) High-magnification High-angle annular dark-field STEM image showing the {11$\bar{2}$1} TB at the atomic scale. (e) Schematic diagram of the structure of the {11$\bar{2}$1} TB.

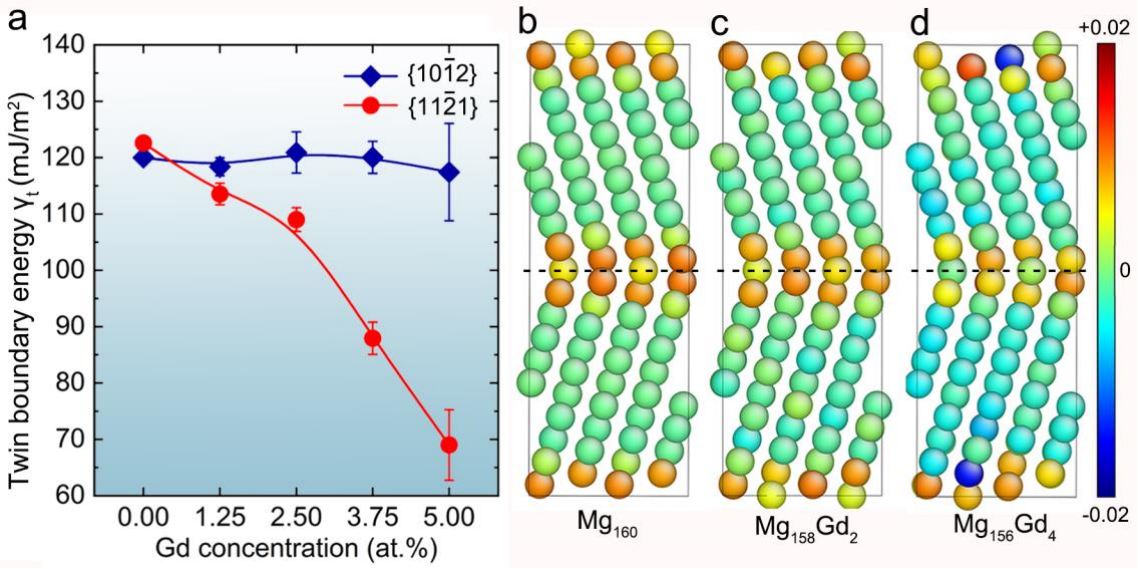

Fig. 3. (a) DFT-calculated TB energies (γ_t) values with different Gd concentrations in the α-Mg solid solution, based on the special quasirandom structure (SQS) formalism. (b-d) Variation of the atomic local strain hydrostatic invariant (ALSHI) in {11$\bar{2}$1} TB with different Gd concentration in the α-Mg solid solution: (a) Pure Mg, (b) $Mg_{158}Gd_2$, (c) $Mg_{156}Gd_4$. Extension strain and compression strain in each atomic site are colored by red and blue, respectively.

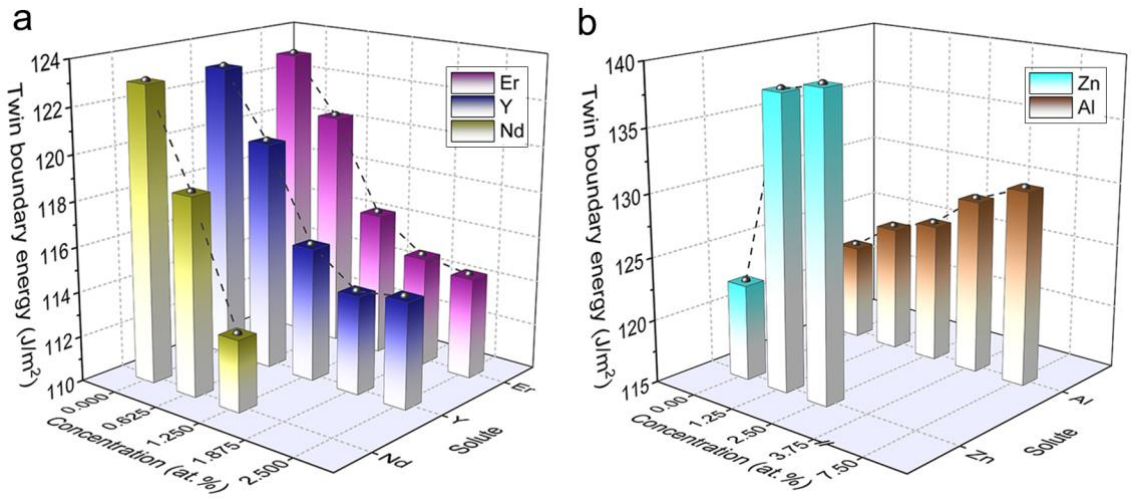

Fig. 4. DFT-calculated $\{11\bar{2}1\}$ TB energies for other solutes with various concentrations in the α-Mg solid solution. Larger solute atoms (Er, Y and Nd) decrease the $\{11\bar{2}1\}$ TB energies while smaller solute atoms (Zn and Al) would increase the TB energy.